Angular dependence of multiple-electron capture in 90-keV Ne^{7+}-Ne collisions

H. Schmidt-Böcking*† and M. H. Prior
Materials and Chemical Sciences Division, Lawrence Berkeley Laboratory, University of California, Berkeley, California 94720

R. Dörner and H. Berg
Institut für Kernphysik, Universität Frankfurt, D-6000 Frankfurt am main 90, August-Euler-Strasse 6, Federal Republic of Germany

J. O. K. Pedersen
Institute of Physics, University of Aarhus, DK-8000 Aarhus C, Denmark

C. L. Cocke and M. Stockli
Department of Physics, Kansas State University, Manhattan, Kansas 66506

A. S. Schlachter
Accelerator and Fusion Research Division, Lawrence Berkeley Laboratory, University of California, Berkeley, California 94720
(Received 21 December 1987)

Multiple-electron capture as a function of the projectile scattering angle in 90-keV Ne^{7+} collisions on Ne atoms was investigated in the angular range from 1 to 20 mrad by a recoil-ion–projectile coincidence technique which records the final charge states of both product ions. A single-electron-capture probability $P_{SC}(\theta)$ is determined, which, with application of binomial statistics, provides a good description of measured charge-state distributions for $\theta < 10$ mrad. For scattering angles $\theta > 10$ mrad, projectile and recoil-ion charge-state distributions are nearly identical, indicating full participation of all L-shell electrons in quasimolecular states. Nearly all electron-capture processes are followed by autoionization, indicating the importance of capture into multiply excited states. We observed a strong angular dependence of the autoionization probabilities.

I. INTRODUCTION

Electron-capture processes in collisions between slow, highly charged ions and atomic targets continue to attract interest.[1,2] Many experimental and theoretical investigations have addressed total electron-capture cross sections (i.e., integrated over all impact parameters), and it has been established by high-resolution Auger electron, x-ray, and projectile energy-gain spectroscopy that single-electron transfer from the atom to the projectile ion is very final-state selective.[3–11] This observation is often explained by the static "classical over barrier model."[12–15] In this model, electron transfer can occur when the Coulomb barrier "seen" by the active electron becomes low enough to allow it to move classically between the collision partners. This occurs at an internuclear separation which depends upon the projectile charge and the binding energy of the electron in the atom. For the case of multiple-electron capture, the electrons are transferred at different internuclear separations R_m, which decrease with increasing number m of captured electrons. This picture implies that multiple-electron capture should depend strongly upon the projectile scattering angle θ. The multiple-capture probability $P_{MC}(\theta)$ should increase strongly with increasing θ (decreasing impact parameter).

Only a few experimental studies to date have been performed which measure the angular dependence of the single- and multiple-electron-capture processes. Such studies can be made by measuring the projectile final charge and scattering angle in coincidence with the final charge-state-analyzed recoil ion from the atomic target.[16–18] The state into which the electron is captured can be determined[17] in addition by use of high-resolution translational spectroscopy on the projectile product. For multiple-electron transfer, however, many states are involved which are unresolved by the technique. These first measurements, indeed, demonstrated that the angular-dependent probabilities shifted to larger scattering angles with increasing number of captured electrons. We report here measurements for 90-keV Ne^{7+} on Ne atoms, where the angular dependence for transfer of one to six electrons has been investigated. We have used a projectile–recoil-ion coincidence with position-sensitive detection of the final projectile charge states and scattering angles. Flight time determines the recoil-ion charge state, and charge balance yields the number of electrons "lost" in the collision.

Although at present no theoretical description of the angular dependence of multiple-electron capture is available for our system, we infer from the symmetry of the projectile and recoil-ion charge-state distributions for scattering angles $\theta > 10$ mrad that a complete quasi-

molecular system is formed populating the target and projectile final states with equal probability. A scattering-angle-dependent single-electron-capture probability is derived, from which the measured charge distributions are calculated using binomial statistics. For $\theta < 10$ mrad, projectile and target products have different (nearly complementary) charge-state distributions, and autoionization makes a very different contribution to the two distributions.

II. EXPERIMENTAL ARRANGEMENT

The experiment was performed at Lawrence Berkeley Laboratory using the Electron Cyclotron Resonance (ECR) ion source at the 88-in. cyclotron. A beam of Ne^{7+} was collimated to a beam spot of less than 0.1 mm^2 (see Fig. 1). This beam hit a gas jet target just below the needle from which the gas effused. The target region was buffered from the rest of the beamline by two stages of turbo-molecular pumping (Fig. 1 insert). The inner stage contained a recoil-ion extractor with a uniform electrostatic field ($\approx 50-200$ V/cm) which accelerated the recoil ions into a drift tube, after which the ions were detected by a channel electron multiplier (CEM). Projectile product ions proceeding in the forward direction were deflected an amount proportional to their charge by a transverse electrostatic field (≈ 100 V/cm, along 10 cm of beam path). The deflected projectile product ions were detected by a position-sensitive channel-plate detector (PSD) with a 4-cm-diameter active area. A horizontal slit in front of the deflection plates (see Fig. 1) limited the scattering-angle region (horizontal plane $\theta_{max} \approx 40$ mrad; vertical plane $\theta_{max} \approx 7$ mrad). The angular dependence of up to three projectile charge states could be investigated simultaneously. The position-sensitive detector had a two-dimensional, three-electrode, wedge and strip anode structure,[19] from which three charge signals Q_1, Q_2, Q_3, were obtained. Figure 2 shows a schematic of the electronic arrangement. Processing of these signals yielded x and y position information for each projectile detected. A fast time signal from the recoil-ion detector was used to start a time-to-amplitude converter (TAC), which was stopped by the delayed time signal from the projectile detector. Because the recoil ions had low initial velocities and were extracted by an electrostatic field, their time of flight (TOF) into the channeltron detector was proportional to $1/\sqrt{k}$ (k is the recoil-ion charge). Thus we obtained for each true kinematic recoil-ion–projectile coincidence a well-resolved time peak, allowing the determination of k. A drawing of the kinematic coincidence is shown in Fig. 3. Each data event was collected by a computer system and saved on magnetic tape for off-line analysis.

The measurements were performed at different target pressures to ensure single-collision conditions. The typical pressure in the second pumping stage was in the order of 1×10^{-6} torr, the pressure in the beam line in front of the target $(2-3) \times 10^{-7}$ torr. To make an x-y position calibration the detector could be covered with a grid. The shadow structure of this grid was observed by "illuminating" the detector with a broad beam from a small Cs^+ ion source mounted below the Ne^{7+} beam axis.

III. DATA ANALYSIS

Each four-parameter event (Q_1, Q_2, Q_3, TOF) was transformed into three parameters (x,y,TOF). For the two-dimensional anode used (Ref. 19) the coordinates x and y were derived from the relations $x = Q_1/\sum Q$ and $y = Q_3/\sum Q$, where $\sum Q = Q_1 + Q_2 + Q_3$. Only such events were analyzed where $\sum Q$ was clearly separated from noise signals present in the channel-plate system. Thus the noise background (typically a few percent of the real scattering yield) was nearly completely eliminated. Figure 4 shows an example of the x-y position data for

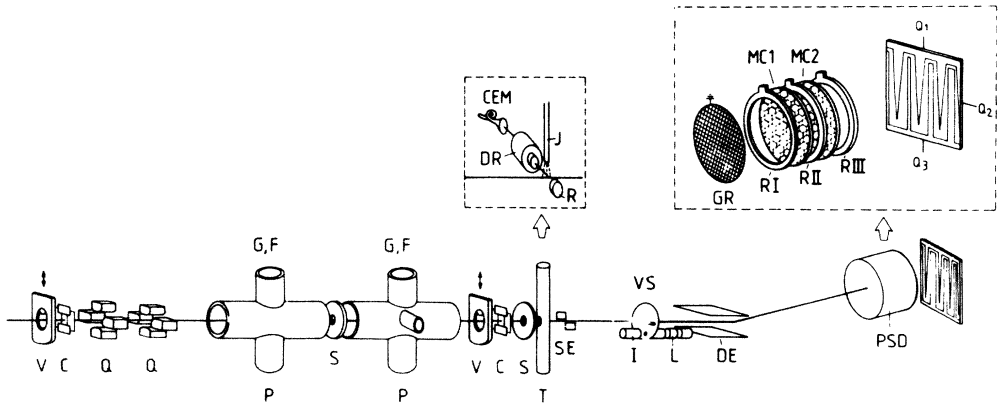

FIG. 1. Experimental arrangement: the charge-state analyzed ion beam from the ECR source moves from left to right. V, valve; C, four-jaw collimator; Q, electrostatic quadrupole; P, pump position; G, ion gauge; F, Faraday cup; S, aperture; T, two-stage differential gas target system (insert shows recoil-ion spectrometer: CEM, channeltron detector; DR, recoil-ion drift tube; J, gas jet; R, repeller electrode); SE, compensating electrostatic deflectors; VS, vertical slit; I, cesium ion source; L, einzel lens; DE, electrostatic deflectors to separate projectile charge states; PSD, position sensitive channel-plate detector (insert shows: GR, grid; R I, R II, R III, potential rings; MC1,MC2, microchannel multiplier plates; Q_1, Q_2, Q_3, wedge and strip anode electrodes.

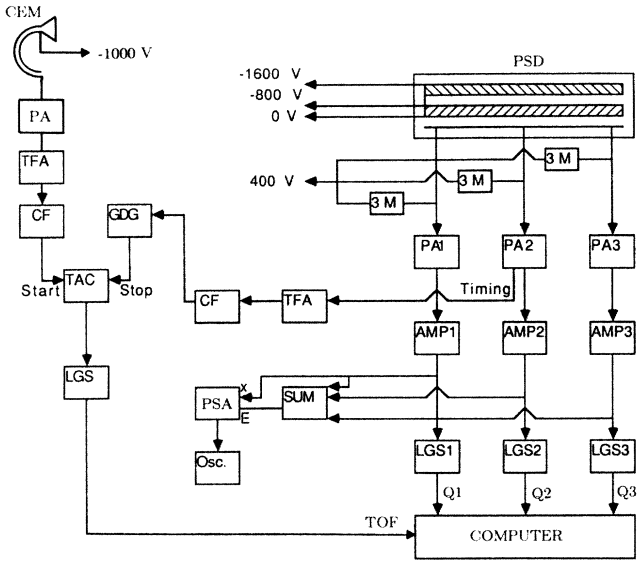

FIG. 2. Block diagram of the electronic arrangement. CEM, channel electron multiplier; PSD, position-sensitive particle detector, $3M=3\times10^6$-Ω resistor; PA, preamplifier; TFA, timing filter amplifier; CF, constant fraction discriminator; GDG, gate and delay generator; TAC, time-to-amplitude converter; LGS, linear gate and stretcher; SUM, summing amplifier; PSA, analog position analyzer; Osc, oscilloscope; $[Q_1,Q_2,Q_3,\text{TOF}]$, four-parameter event signal.

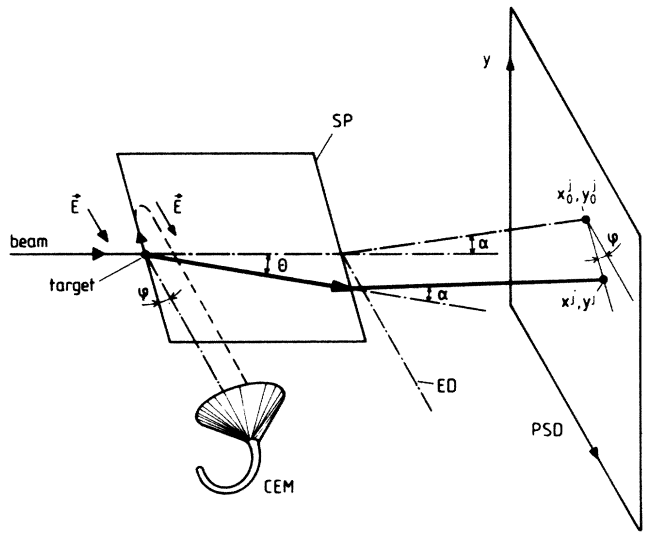

FIG. 3. Sketch of the target recoil ion, projectile product ion coincidence geometry. SP, scattering plane; θ, scattering angle; α, angle of electrostatic deflection of projectile in charge state j; ED, position of electrostatic deflector; x_0^j,y_0^j, coordinates of projectile in charge state j and deflection $\theta=0°$; x^j,y^j, coordinates of scattered projectile on position-sensitive channel-plate detector (PSD). E, electrostatic field in target region to collect recoil ions into channeltron detector (CEM). The dashed line represents the trajectory of an extracted recoil ion with an initial velocity component in the (−) direction (see text).

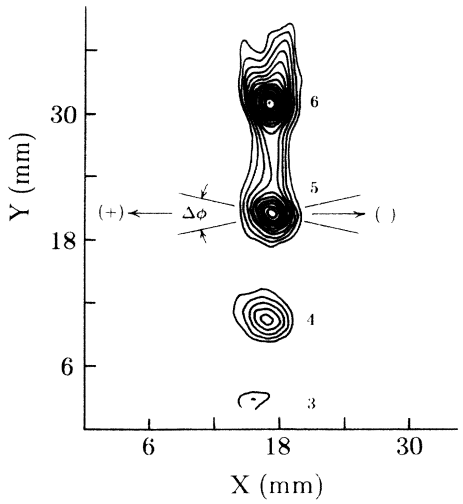

FIG. 4. Example of x-y position data for projectile product charge states 6 + , 5 + , 4 + . This is a "singles" spectrum, that is, it is not sorted according to coincident recoil-ion charge states produced. The contours are at logarithmic intervals corresponding to a decrease in intensity by a factor of ≈0.56 in the direction away from each spot center. One notes the decreased rate of fall of intensity with distance (proportional to scattering angle) for the lower charge projectile products. The directions (+) and (−) correspond to target ion recoil directions parallel and antiparallel to the extraction field, respectively, in the recoil-ion spectrometer (see Fig. 3). Scattering angle dependence of the charge transfer events is obtained by integrating over the azimuthal angle ϕ in the range $\Delta\phi=26°$, centered on the (+) direction. Distortion of the contours near the top of the plot is due to proximity to the edge of the position-sensitive detector.

projectile product charges 6+, 5+, 4+ (a weak 3+ signal is present also). The data shown is a "singles" spectrum, that is, it includes all recoil-ion charge states. The data are processed by locating the center of each projectile product spot and transforming each x-y event position into θ,ϕ, where θ is the projectile scattering angle (given by the distance from the spot center divided by the path length to the detector) and ϕ is an azimuthal angle measured from a line through the center in the $+y$ direction. The directions (+) and (−) in Fig. 4 indicate projectile scattering events in which target product ions recoil parallel or antiparallel, respectively, to the extraction electric field in the recoil spectrometer (see Fig. 3).

The recoil-ion spectrometer consists of a uniform extraction field extending a distance $s_0\approx1$ cm from the gas jet, followed by an equipotential drift region of length $s_1\approx2$ cm, followed by the channel electron multiplier. The gas jet is held at ground potential, and the field is produced by application of potentials $+V$ and $-V$ to plane electrodes separated by $2s_0$ (V was typically 200 V). The time to traverse the distance to the detector for an ion of charge $+k$, mass m, starting near the jet and moving with initial kinetic energy E_R parallel or antiparallel to the extraction field is given by

$$T_k=t_kf_k\ , \tag{1a}$$

where

$$t_k = \left[\frac{2ms_0^2}{eVk}\right]^{1/2}, \tag{1b}$$

$$f_k = 1 + \frac{s_1}{2s_0} - (\pm)\epsilon^{1/2} + \tfrac{1}{2}(\epsilon+\delta)\left[1 - \frac{s_1}{2s_0}\right], \tag{1c}$$

and

$$\epsilon = \frac{E_R}{eVk} . \tag{1d}$$

We have allowed the starting position to be at a distance $s_0(1+\delta)$ from the $-V$ electrode. The positive (negative) sign is for the case of parallel (antiparallel) recoil. The formula above is valid for the case $\epsilon, \delta \ll 1$ and, as is well known, the case where $s_1 = 2s_0$ removes the leading dependence on δ. For this case one has

$$T_k = 2t_k - (\pm)t_1 \left[\frac{E_R}{eV}\right]^{1/2} \frac{1}{k} . \tag{2}$$

If one neglects momentum lost to photons and to electrons emitted from the collision, then, for equal target and projectile masses,

$$E_R = \theta^2 E_P , \tag{3}$$

where E_P is the projectile energy. Thus

$$T_k = 2t_k - (\pm)t_1 \left[\frac{E_P}{eV}\right]^{1/2} \frac{\theta}{k} . \tag{4}$$

Figure 5 shows a plot of θ versus T_k for both $(+)$ and $(-)$ cases for collisions producing a $4+$ projectile product. The lines are drawn to show the dependence of T_k on θ for each k value. One sees that there is agreement with the predictions of Eq. (4) for $k = 3,4,5$ but not for $k = 1,2$. These latter cases are not primary recoil events, however, since, by charge balance, they cannot be produced by a projectile charge change $7+ \rightarrow 4+$. The apparent $1+$ and $2+$ recoil products are produced by secondary charge-transfer collisions of higher charged primary recoil ions with target gas atoms and the surface of the gas jet needle. The near vertical orientation of the contours for the $1+$, $2+$ ions is indicative of their low-velocity origin (near the thermal velocity of the target gas), and is in marked contrast with the orientation of the $3+$, $4+$, $5+$ recoil events. From these two dimensional data (θ, T_k) the relative differential scattering cross section $\Delta\sigma_{\rm rel}(j,k,\theta)/\Delta\theta$ is obtained. (Throughout this work j denotes a projectile final charge state and k denotes a recoil-ion charge state.) This is done by extracting the number of events as a function of θ along the (θ, T_k) trajectories such as shown in Fig. 5, for each value of k. Only the $(+)$ trajectories are used because the recoil spectrometer has an efficiency which varies significantly with θ for the $(-)$ case, due to recoil velocity components transverse to the extraction field. Because in the data reduction $\Delta\phi = \text{const}$ these $\Delta\sigma_{\rm rel}/\Delta\theta$ are related to $\Delta\sigma_{\rm rel}/\Delta\Omega$ by

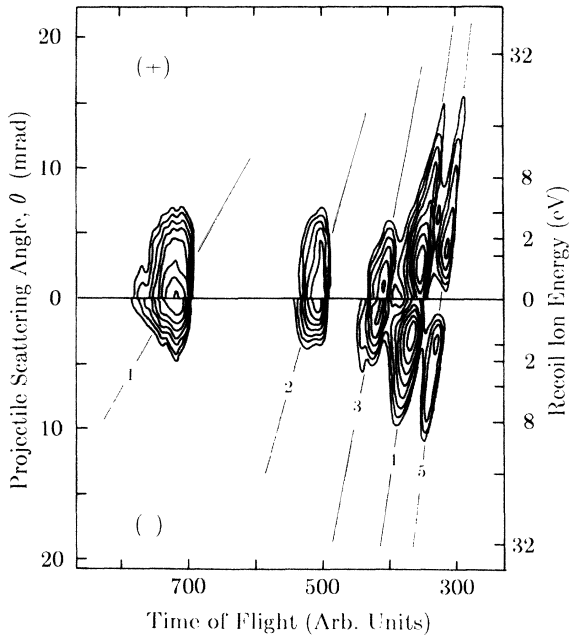

FIG. 5. Scattering angle θ vs time of flight T_k for recoil ions in coincidence with projectile product charge state $4+$. The contours are at logarithmic intervals corresponding to a factor of ≈ 0.59. The lines are the predictions of Eq. (4). Recoil products $3+$, $4+$, $5+$ arise from the primary collision, apparent recoils with charge $1+$ and $2+$ are secondary products from electron capture collision of the primary recoil ions with target atoms and surfaces. The energy scale on the right is derived from Eq. (3). The upper $(+)$ and lower $(-)$ halves of the figure are constructed from events with recoil ions moving initially parallel and antiparallel, respectively, to the extraction field in the time-of-flight spectrometer. The $(+)$ and $(-)$ data were computer processed separately; this accounts for the discontinuity in the contours across the $\theta = 0$ line.

$$\frac{\Delta\sigma_{\rm rel}}{\Delta\Omega} = \frac{\Delta\sigma_{\rm rel}}{\Delta\theta}\frac{1}{\Delta\phi\sin\theta} . \tag{5}$$

Since not all $j = 6, \ldots, 1$ could be detected simultaneously on the PSD (usually three adjacent projectile product charge states struck the detector), several runs with different j detected were performed. These sets of data were easily normalized to each other because, in each run, at least one j was common with a previous measurement. For example, data taken with charge states $6+$, $5+$, $4+$ present were normalized to data with $4+$, $3+$, $2+$ present via the common $4+$ events.

IV. EXPERIMENTAL RESULTS AND DISCUSSION

All measured relative differential cross sections $\Delta\sigma_{\rm rel}(j,k,\theta)/\Delta\theta$ are presented in Fig. 6, normalized to the total number of events. Because they were obtained in different runs, higher cross sections can have poorer statistics and therefore larger statistical error (dashed area) than lower cross-section cases, where more events were recorded. Table I lists the j,k combinations measured. Since the projectile and recoil ions are detected

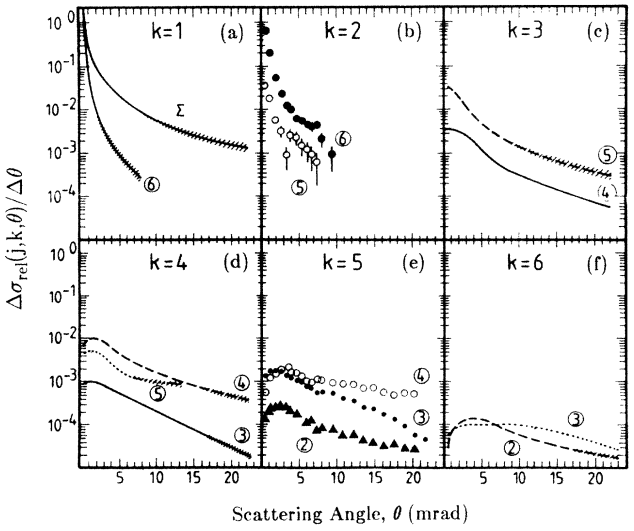

FIG. 6. Relative differential cross sections $\Delta\sigma_{rel}(j,k,\theta)/\Delta\theta$. j, final projectile charge state after collision; k, final recoil charge state after collision. Values of j are denoted by the circled numbers. For most cases lines have been drawn through the experimental data points, smoothing out statistical fluctuations. The hatched areas along the curves indicate the statistical spread of the data where it is significant. Sample data are shown for cases $k=2$ and $k=5$.

and separated according to their final charge states at a time $>10^{-6}$ sec after the collision, the measured data are influenced by autoionization of ions in multiply excited final states. This effect shifts the measured coincident charge-state distributions generally to higher charge.

To gain a better understanding of the multielectron capture process the data in Fig. 6 are presented as different reduced quantities. The total reaction scattering yield

$$\frac{\Delta\sigma_{tot}}{\Delta\theta}=\sum_{j,k}\frac{\Delta\sigma_{rel}(j,k\theta)}{\Delta\theta} \tag{6}$$

is calculated (labeled Σ in Fig. 6) to obtain relative capture probabilities. The θ dependence of the total yield for $\theta>3$ mrad is much weaker than Rutherford scattering, which is expected for these small-angle collisions, where screening is important. The steep θ dependence observed for $\theta<3$ mrad is partially due to an uncertainty in the θ calibration in this range because of the finite size of the beam; only the relative probabilities will be considered in this region.

TABLE I. Matrix of final projectile j and recoil ion k charge-state pairs for which scattering data have been obtained. The entries are the number of lost electrons.

j \ k	6	5	4	3	2	1
6	·	·	·	·	1	0
5	·	·	2	1	0	
4	3	2	1	0		
3	2	1	0			
2	1	0				

The relative fractions [probabilities $P(j,\theta)$ and $P(k,\theta)$] for the projectile and recoil-ion products, respectively, are presented in Figs. 7(a) and 7(b). The figures are derived from the data of Fig. 6 by summing over, respectively, all recoil and all projectile charge states and dividing by $\Delta\sigma_{tot}/\Delta\theta$. If autoionization did not occur, both data sets would directly reflect the angular dependence of the multiple-capture differential cross sections and the sets should be complementary.

Calculation of the mean recoil-ion charge $\bar{k}(\theta)=\sum_k kP(k,\theta)$ and mean projectile product charge $\bar{j}(\theta)=\sum_j jP(j,\theta)$ allows determination of the total mean charge $\bar{Q}(\theta)=\bar{k}(\theta)+\bar{j}(\theta)=7+\bar{\eta}(\theta)$, where $\bar{\eta}(\theta)$ is the number of missing electrons per collision. Figure 8 shows $\bar{j}(\theta)$, $\bar{k}(\theta)$, and $\bar{\eta}(\theta)$. It is seen that $\bar{\eta}$ increases slightly with angle and is, for all θ, close to one; i.e., on average, the collisions are followed by one autoionization process. As listed in Table I, double autoionization occurred in three observed cases and, although only weakly

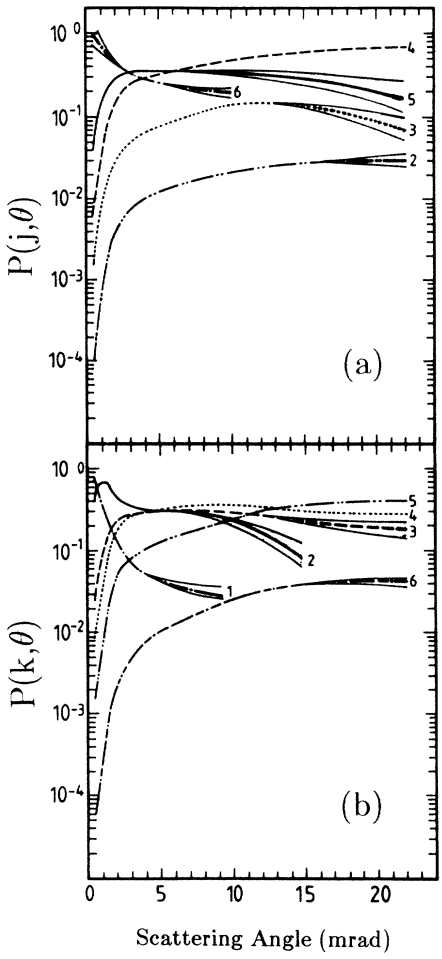

FIG. 7. (a) Relative projectile differential probability $P(j,\theta)$ and (b) recoil-ion differential probability $P(k,\theta)$. The curves are labeled by projectile-ion final charge j and recoil-ion charge k, respectively.

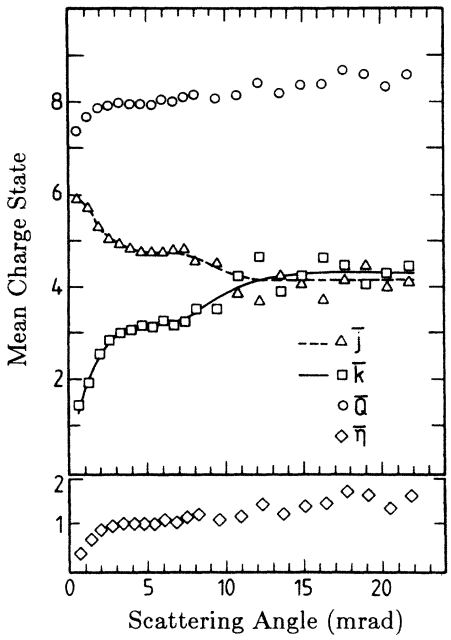

FIG. 8. Mean recoil charge states $\bar{k}(\theta)$, mean projectile charge state $\bar{j}(\theta)$, and mean total charge $\bar{Q}(\theta)$. $\bar{\eta}(\theta)$ is the mean number of electrons emitted per collision by autoionization.

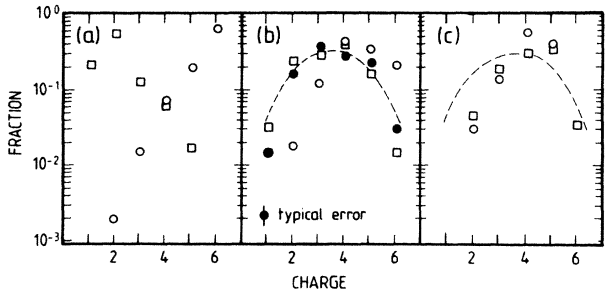

FIG. 9. Charge-state distributions of recoil ions (squares) and projectile ions (open circles) at scattering angles (a) $\theta=1.5$ mrad, (b) $\theta=8.0$ mrad, and (c) $\theta=16$ mrad. The dashed line is the result from the semiempirical calculation using the single-electron-capture probability measured here (see text) and assuming a binomial distribution. The solid circles represent the instantaneous projectile charge-state distribution (prior to subsequent autoionization), defined as the recoil distribution reflected about charge 3.5.

detected, there was evidence for triple autoionization in one instance. We observe from Fig. 8 that, indeed, $\bar{j}$ and $\bar{k}$ are approximately complementary. However, for larger angles, $\theta \geq 12$ mrad, both approach the same equilibrium value, indicating that projectile and target shells significantly mix their electrons in such close symmetric Ne-Ne collisions, forming, for all L-shell electronic states, a complete quasimolecular system.

Since seven electrons can be transferred between the collision partners, $\bar{k}(\theta)/7 \equiv P_{SC}(\theta)$ is the single-electron-capture probability if the electrons are captured independently and any small autoionization contribution in the recoil charge-state distribution is neglected. Using binomial statistics the multiple (k) electron-capture probability is then

$$P_k(\theta)=\begin{bmatrix}7\\k\end{bmatrix}P_{SC}^k(\theta)[1-P_{SC}(\theta)]^{7-k}\,. \tag{7}$$

The experimental charge distributions for the recoil and projectile ions are shown in Fig. 9 for scattering angles $\theta=1.5$, 8, and 16 mrad, revealing some interesting aspects of the electron capture and autoionization process in this collision system. We first discuss the recoil-ion and projectile product charge distributions at $\theta=8$ mrad. The recoil-ion distribution is wider and more symmetric around $\bar{k}=\frac{7}{2}$ than the projectile distribution, which is shifted to higher charge. One sees in Fig. 8 that at $\theta \approx 8$ mrad, $\bar{k}(\theta)$ approaches the maximum mean capture value of $\frac{7}{2}$, which implies that $P_{SC}=0.5$. Assuming that the recoil ion is not multiply excited (i.e., it cannot autoionize) for $\theta < 8$ mrad, we can calculate the recoil-ion distribution [dashed line in Fig. 9(b)] using $P_{SC}=0.5$ in Eq. (7). This binomial distribution is a good description of the measured values. Assuming that $\bar{\eta}$ ($\theta=8$ mrad) arises only from projectile autoionization, one can define the instantaneous projectile distribution (that is the distribution before autoionization events) from the recoil-ion distribution reflected about charge 3.5. This is shown in Figure 9 as the solid circles. One notes that the measured projectile fractions (open circles) are nearly identical to the instantaneous fractions provided that the latter are shifted one charge unit higher. Thus we conclude that, at $\theta=8$ mrad, the target and projectile have shared completely their L shell electrons; however, only the projectile remains in a multiply excited state. This is in agreement with conclusions from other measurements.[10,20,21]

The measured recoil-ion and projectile product distributions at $\theta=16$ mrad [Fig. 9(c)] agree within their error limits. However, the experimental distributions appear narrower than the binomial prediction (dashed line) and are shifted to a higher charge state. As will be shown below, for $\theta > 10$ mrad, electrons and vacancies can be shared between both partners via the quasimolecular $4f\sigma$ promotion, leading to autoionization in either (or both). This explains why the distributions are essentially the same. Since the relative importance of autoionization depends on the number of possible excited electrons, it is much more important on the low-charge side of the distributions. This may explain the narrowing.

The complete statistical sharing of all target L electrons between the projectile and target is expected, in the framework of quasimolecular formation, to begin approximately at a distance of closest approach for which the $4f\sigma$ orbital is promoted. According to molecular-orbital (MO) calculations of Wille[22] for the Ne^{7+} on the Ne system, this is expected to occur near an internuclear distance R of about 0.5 a.u. (see Fig. 10). That this distance is not very dependent on charge states of the collision partners is seen in Fig. 10 by comparing the results for Ne^{7+} on Ne^{0+} with those for Ne^{4+} on Ne^{3+}. The scattering angle which would result from a collision penetrating to this internuclear distance can be estimated from the scattering angle which would result from two

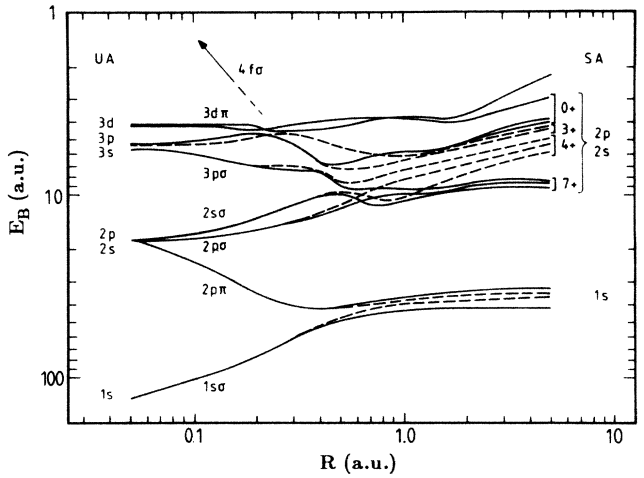

FIG. 10. Quasimolecular correlation diagram, binding energy E_B vs internuclear separation R, for Ne^{7+} on Ne^{0+} (solid lines) and for Ne^{4+} on Ne^{3+} (dashed lines) from Ref. 22. Note that the regions of coupling to the $4f\sigma$ orbital do not vary markedly with the partition of charge among the partners. The united atom UA and separated atom SA levels are listed on the left and right.

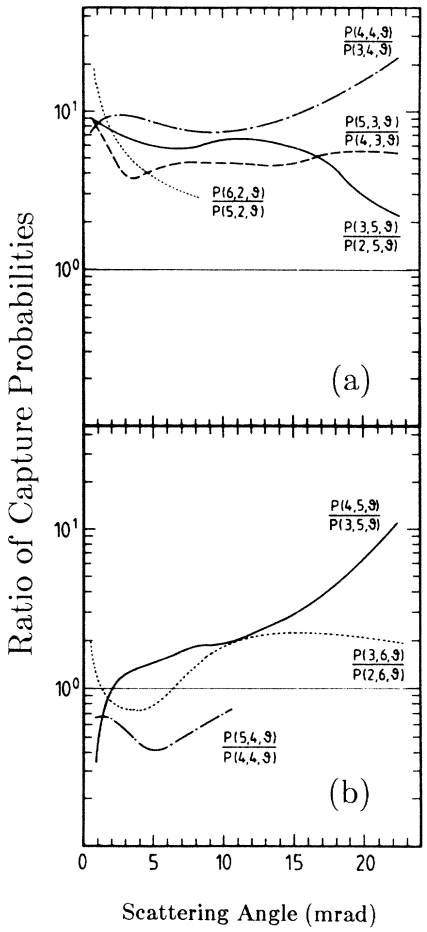

FIG. 11. Ratios of electron-capture probabilities, $P(j',k,\theta)/P(j,k\theta)$, vs scattering angle for projectile final charge j', recoil-ion charge k to projectile final charge j, recoil-ion charge k. (a) shows the ratios for one electron lost ($j'+k=8$) to zero electrons lost ($j+k=7$). (b) shows the ratios for two electrons lost ($j'+k=9$) to one electron lost.

Ne^{4+} projectiles which change from a straight-line trajectory to a Coulomb trajectory at a distance of closest approach of 0.5 a.u. For 90-keV projectiles, this angle is 5 mrad, slightly smaller than that for which we observe quasimolecular L vacancy sharing to proceed. Since some deflection occurs before the distance of closest approach is reached, and appreciable sharing will be realized only for collisions which penetrate substantially inside this minimum R, it is not surprising that the observed angle of 8–10 mrad for which sharing becomes large lies somewhat outside that obtained from this simple estimate.

For smaller scattering angles, i.e., larger R_0, the simple classical barrier model predicts that the projectile can only capture electrons into an excited state and that the remaining target L electrons will hardly be excited. This expectation can be tested when electron-capture processes followed by single ($\eta=1$) and double ($\eta=2$) autoionization are investigated. Single autoionization can only occur if at least two electrons are captured into an excited state since, at larger R, additional core excitation in the projectile or target can be excluded. Double autoionization at large R can occur only when four electrons are captured into an excited state (4 in the projectile, or 2 in the projectile and 2 in the recoil). Indeed, for $k \leq 1$ no autoionization, for $k \leq 3$ no double autoionization, and for $k \leq 5$ no triple autoionization was observed above experimental backgrounds, in agreement with the above discussed expectations. Only for $k=6$ (see Table I) has triple autoionization been weakly observed.

The ratios of the electron-capture probabilities, $P(j',k,\theta)/P(j,k,\theta)$, are plotted in Fig. 11. These probabilities are the normalized relative cross sections shown in Fig. 6. Figure 11(a) contains the ratios of probabilities for single to zero autoionization. The case of $k=2$ shows a surprising dependence; the ratio is strongly decreasing with increasing θ. For increasing angle, one electron seems to be captured with growing probability into low-lying projectile states, closing the autoionization channel. If more than two electrons are captured, the autoionization channels are by far the dominant ones, and the ratios are nearly constant over a wide angular range. Only for larger angles ($R<0.5$ a.u.) do these ratios vary with angle, because (as discussed above) the L shells are strongly coupled and L electrons can be promoted or demoted to all states above the $2s$ level.

The ratios of double ($\eta=2$) to single ($\eta=1$) autoionization in the final state following electron capture are shown in Fig. 11(b); very strong variation with θ is observed. The reduced double-ionization probability for $k=4$ and 6 around $\theta \approx 5$ mrad remains unexplained. Obviously, again, at least one electron is captured into a low-lying state. Towards large θ the excitation into higher states strongly increases, and, for θ greater than about 10 mrad, extends to both collision partners. The low double-autoionization probability for $k=4$ is expected because here all four electrons must be captured into excited states.

Finally, we point out that the simple relation, Eq. (3), allows one to convert the angular scattering data into recoil-ion transverse energy distributions for each of the final target and projectile states. Furthermore, calculation of the mean value of θ^2 yields, via Eq. (3), the mean recoil-ion energy transverse to the projectile beam. Figure 12 shows a plot of these mean values versus recoil-ion charge, where we have distinguished between cases of 0, 1, and 2 electrons lost. One sees that the points fall along approximately the same line regardless of the number of lost electrons. The mean energy increases as approximately the 2.6 power of the recoil charge.

It is true, of course, that Eq. (3) is only valid provided one can neglect momentum carried away by photons and electrons emitted during or after the collision. Photons carry away insignificant momentum, so one is concerned with sharing among lost electrons and the target recoil ions. For the case where no electrons are lost, one can assign the momentum entirely to the recoil ions and Eq.(3) yields their transverse energy. In fact, two-body kinematics predicts that Eq. (3) gives the *total* recoil energy as long as θ^2 and E_Q/E_P are small; E_Q is the potential energy liberated in the collision. These conditions are satisfied for the reactions studied in this work. For cases where electrons are lost, if one assigns all the transverse momentum to one electron, this would yield an electron energy of about 3.6 keV for $\theta=1$ mrad, and much more for the larger scattering angles. Since it is unreasonable to expect electron energies of this magnitude we feel justified in assigning the projectile product transverse momentum to the recoiling target ion. We point out that direct measurement of such low recoil-ion energies is very difficult and rare in the literature.[23–25]

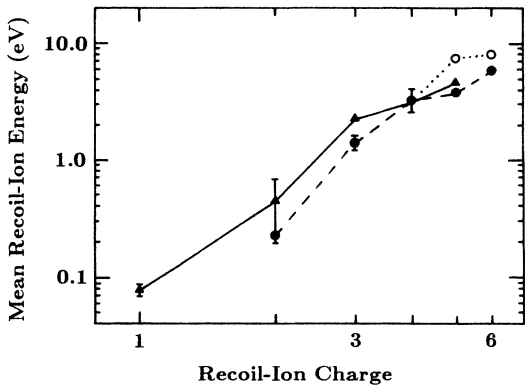

FIG. 12. Mean recoil-ion energies vs recoil charge. Triangles, solid circles, and open circles are for collisions followed by zero, one, and two electron loss (autoionization), respectively.

V. CONCLUSION

We have observed capture of up to six electrons per encounter by the highly charged projectile in 90-keV Ne^{7+} on Ne collisions. We infer that generally the capture occurs predominantly into multiply excited states and thus is nearly always followed by autoionization. The data show that the excitation probability into these states varies strongly with scattering angle. For $\theta \geq 8$ mrad, projectile and recoil-ion L electron shells form a quasimolecular system, completely sharing these electrons, which leads to nearly identical charge-state distributions. An electron-capture probability, $P_{SC}(\theta)=\bar{k}(\theta)/7$ is extracted from the data, which, using binomial statistics, provides a fairly good description of the measured recoil-ion charge-state distributions for $\theta \leq 8$ mrad. A parameter-free theoretical description is not available, in part because, at this velocity in the multielectron system, electron screening has a very strong influence on the capture and scattering process. We point out that recoil-ion transverse-energy distributions can be obtained by a simple transformation of the scattering angle data, and we observe, from such a treatment, that the mean recoil-ion energy increases with approximately the 2.6 power of the recoil-ion charge for this collision system. Finally, we express the hope that these experiments will help to stimulate more theoretical activity on the angular dependence of multielectron-capture processes.

ACKNOWLEDGMENTS

The authors acknowledge the assistance and hospitality of Dr. C. Lyneis, Dr. R. Stokstad, and other members of the Lawrence Berkeley Laboratory (LBL) 88-inch Cyclotron staff. Particular thanks go to the workshops at LBL, Kansas State University, and Universität Frankfurt. Important parts of the apparatus were transported from Frankfurt to San Francisco through the generosity of Lufthansa. Support for this work was provided by the Director, Office of Energy Research, Office of Basic Energy Sciences, Chemical Sciences Division, U.S. Department of Energy (M.H.P., H.S.-B., C.L.C., M.S., R.D., J.O.K.P.), Kansas State University (H.S.-B., C.L.C., M.S.), the Deutsche Forschungsgemeinschaft (H.S.-B., R.D., H.B.), and NATO (J.O.K.P.). Additional support was provided by the Friedrich Ebert Stiftung (R.D.) and NATO Research Grant No. 0501/85 (H.B.).

*On leave from Department of Physics, Kansas State University, Manhattan, KS 66506.

†Permanent address: Institut für Kernphysik, Universität Frankfurt, D-6000 Frankfurt am main 90, August-Euler-Strasse 6, Federal Republic of Germany.

[1]R. K. Janev and H. P. Winter, Phys. Rep. **117**, 265 (1985).

[2]W. Fritsch, Proceedings of the International Conference on Highly Charged Ions, Groningen, The Netherlands [Nucl. Instrum. Methods B **23**, 9 (1987), and numerous references therein.

[3]R. Mann, H. F. Beyer, and F. Folkmann, Phys. Rev. Lett. **46**, 646 (1981).

[4]R. Mann, C. L. Cocke, A. S. Schlachter, M. Prior, and R. Marrus, Phys. Rev. Lett. **49**, 1329 (1982).

[5]Y. S. Gordeev, D. Dijkamp, A. G. Drentje, and F. J. de Heer, Phys. Rev. Lett. **50**, 1842 (1983).

[6]F. Folkmann, K. M. Cramon, R. Mann, and H. F. Beyer, Phys. Scr. T **3**, 166 (1983).

[7]K. Okuno, H. Tawara, T. Iwai, Y. Kaneiko, M. Kimura, N. Kobayashi, A. Matsumoto, S. Ohtani, S. Takagi, and S. Tsurubuchi, Phys. Rev. A **28**, 127 (1983).

[8]E. H. Nielsen, L. H. Andersen, A. Barany, H. Cederquist, J. Heinemeier, P. Hvelplund, H. Knudsen, K. B. MacAdam, and J. Sorensen, J. Phys. B **18**, 1789 (1985).

[9]F. W. Meyer, A. M. Howald, C. C. Havener, and R. A. Phaneuf, Phys. Rev. Lett. **54**, 2663 (1985).

[10]A. Bordenave-Montesquieu, P. Benoit-Cattin, M. Boudjema, A. Gleizes, and S. Dousson, Nucl. Instrum. Methods B **23**, 94 (1987).

[11]M. Mack, Nucl. Instrum. Methods B **23**, 74 (1987).

[12]H. Ryufuku, K. Sasaki, and T. Watanabe, Phys. Rev. A **21**, 745 (1980).

[13]R. Mann, F. Folkmann, and H. F. Beyer, J. Phys. B **14**, 1161 (1981).

[14]A. Barany, G. Astner, H. Cederquist, H. Danared, S. Huldt, P. Hvelplund, A. Johnson, H. Knudsen, L. Liljeby, and K. G. Rensfelt, Nucl. Instrum. Methods B **9**, 397 (1985).

[15]A. Niehaus, J. Phys. B **19**, 2925 (1986).

[16]P. Roncin, M. N. Gaboriaud, H. Laurent, and M. Barat, J. Phys. B **19**, L691 (1986); see also M. Barat, H. Laurent, M. N. Gaboriaud, L. Guillemot, and P. Roncin, in *Invited Papers of the Fifteenth International Conference on the Physics of Electron and Atomic Collisions, Brighton, United Kingdom, 1987,* edited by H. B. Gilbody, W. R. Newell, F. H. Read, and A. C. H. Smith (North-Holland, New York, 1988), p. 613.

[17]H. Laurent, P. Roncin, M. N. Gaboriaud, and M. Barat, Nucl. Instrum. Methods B **23**, 45 (1987).

[18]H. Danared, H. Andersson, G. Astner, A. Barany, P. Defrance, and S. Rachafi, J. Phys. B **20**, L165 (1987); Phys. Scr. **36**, 756 (1987).

[19]C. Martin, P. Jenlinsky, M. Lampton, R. F. Malina, and H. O. Anger, Rev. Sci. Instrum. **52**, 1067 (1981).

[20]R. Mann and H. Schulte, Z. Phys. D **4**, 343 (1987).

[21]M. Mack, A. G. Drentje, and A. Niehaus, *Abstracts of the Fourteenth International Conference of the Physics of Electron and Atomic Collisions, Palo Alto, 1985,* edited by M. J. Coggiola, D. L. Huestis, and R. P. Saxon, (ICPEAC, Palo Alto, 1985), p. 446.

[22]U. Wille (private communication).

[23]J. Ullrich, V. Dangendorf, H. Schmidt-Böcking, S. Kelbch, C. Kelbch, and H. Berg, *Abstracts of the Fifteenth International Conference on the Physics of Electron and Atomic Collisions, Brighton, United Kingdom, 1987,* edited by J. Geddes, H. B. Gilbody, A. E. Kingston, and C. J. Latimer (Queen's University, Belfast, 1987), p. 432.

[24]C.S.O, J. C. Levin, R. T. Short, H. Cederquist, S. B. Elston, J. P. Gibbow, and I. A. Sellin, *Abstracts of the Fifteenth International Conference on the Physics of Electron and Atomic Collisions, Brighton, United Kingdom, 1987,* edited by J. Geddes, H. B. Gilbody, A. E. Kingston, and C. J. Latimer (Queen's University, Belfast, 1987), p. 432.

[25]J. P. Grandin, D. Hennecart, X. Husson, D. Lecler, I. Lesteren-Vaisse, and D. Lisfi, *Abstracts of the Fifteenth International Conference on the Physics of Electron and Atomic Collisions, Brighton, United Kingdom, 1987,* edited by J. Geddes, H. B. Gilbody, A. E. Kingston, and C. J. Latimer (Queen's University, Belfast, 1987), p. 431.